Space Science Reviews (2026) 222:17
https://doi.org/10.1007/s11214-025-01250-x

SPECIAL COMMUNICATION

Geodetic Investigations of the Europa Clipper Mission

G. Steinbrügge[1] · R.S. Park[1] · J.H. Roberts[2] · M. Bland[3] · S. Brooks[1] · J. Castillo-Rogez[1] · G. Cascioli[4,5] · A. Genova[6] · T. Greathouse[7] · H. Hussmann[8] · R. Kirk[3] · A. Magnanini[9] · E. Mazarico[4] · F. Nimmo[10] · M.S. Park[11] · F. Petricca[1] · K. Retherford[7] · D.M. Schroeder[12] · K.M. Soderlund[13] · P. Tortora[9] · M. Zannoni[9]

Received: 27 April 2025 / Accepted: 24 November 2025 / Published online: 3 February 2026

Abstract
The Europa Clipper mission will investigate the geophysical properties of Europa, one of Jupiter's Galilean moons, to assess its habitability. Geodetic measurements will play a critical role in determining Europa's internal structure, including the thickness of the ice shell, the presence and extent of a subsurface ocean, and the distribution of mass in the deeper interior. To build the necessary geodetic data set, the Geodesy Focus Group (GFG) coordinates cross-instrument efforts to measure Europa's global shape, rotational parameters, gravity field, and degree-2 tidal Love numbers (k_2 and h_2). Here we summarize how data from the Gravity/Radio Science (G/RS) investigation, Europa Imaging System (EIS), Radar for Europa Assessment and Sounding (REASON), and Europa Ultraviolet Spectrograph (Europa-UVS) will be used to infer geodetic constraints on the interior structure and to establish a precise cartographic reference system for geophysical and geological interpretation. Together, the resulting geodetic information will contribute to a deeper understanding of Europa's internal dynamics and the potential habitability of its ocean.

1 Introduction

Europa, one of Jupiter's Galilean moons, is a geologically active world, slightly smaller than Earth's moon, and distinguished by its young icy surface and subsurface ocean as indicated by the presence of an induced magnetic field (Kivelson et al. 2000). In combination with intense tidal deformations and the direct ocean-mantle interface, Europa presents a compelling target to understand the potential for life beyond Earth. The primary goal of the Europa Clipper mission is therefore to "Explore Europa to investigate its habitability" (Pappalardo et al. 2024).

Geodetic measurements, which focus on understanding both the static and time-varying geometric shape, orientation in space, and gravitational field, are central to understanding the interior structure and dynamics of Europa. Further, these metrics are critical for constructing a detailed cartographic reference of Europa, which in turn enables the effective combination of different data sets. By combining geodetic data with geophysical observations such as magnetic induction and subsurface radar sounding, the Europa Clipper mission will significantly advance our understanding of Europa's interior (Roberts et al. 2023). This integrated approach, combined with investigations of Europa's geology (Daubar et al. 2024)

Extended author information available on the last page of the article

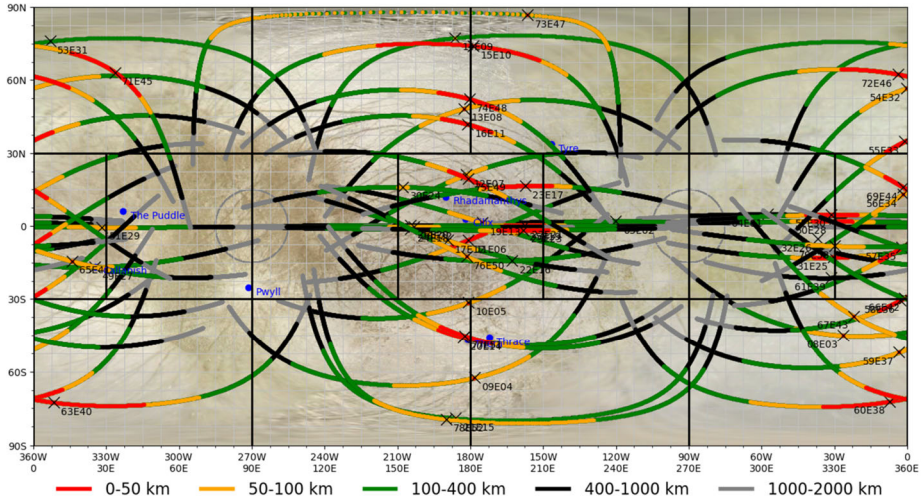

Fig. 1 The Europa Clipper baseline tour[1] shown on a simple cylindrical map projection of Europa's surface centered at 180 degrees longitude. For planning purposes, the surface has been subdivided into 14 panels as outlined by the black lines

and composition (Becker et al. 2024) will fulfill the mission's overarching goal to explore Europa's habitability (Vance et al. 2023).

The Europa Clipper spacecraft carries a suite of complementary instruments that enable highly integrated geodetic investigations of Europa. The role of Europa Clipper's Geodesy Focus Group (GFG) is to coordinate cross-instrument science investigations targeted at determining a common reference frame and providing geodetic constraints for Europa's interior structure. The scientific objectives tracked by the GFG include the determination of Europa's global shape, rotational parameters including librations, the global gravity field, and the degree-2 tidal Love numbers k_2 and h_2.

The main investigations contributing to the geodetic investigations of the Europa Clipper mission are Gravity Radio Science (G/RS; Mazarico et al. 2023), the Europa Imaging System (EIS; Turtle et al. 2024), the Radar for Europa Assessment and Sounding: Ocean to Near-surface (REASON; Blankenship et al. 2024), and the Europa Ultraviolet Spectrograph (Europa-UVS; Retherford et al. 2024).

Europa Clipper's baseline tour design consists of 49 flybys (Fig. 1) distributed over two Europa Campaigns, consisting of 24 and 25 flybys, respectively. Europa Campaign 1 is designed primarily to survey the sun-lit anti-Jovian hemisphere while Europa Campaign 2 focuses on the sun-lit sub-Jovian hemisphere of Europa allowing for excellent coverage across Europa's surface. A notable feature of the tour relevant in particular for the REASON altimetry is that each ground-track crosses at least one other ground-track leading to 141 intersections which can be used to measure the radial tidal deformation of Europa.

In the following we will provide an overview of the state of knowledge of Europa's geodetic parameters (Sect. 2), a description of the datasets with geodetic relevance which will be obtained by the Europa Clipper mission (Sect. 3) and then describe how these datasets work together to infer Europa's geodetic parameters (Sect. 4). Finally, we will dis-

[1] SPICE kernels for the Europa Clipper mission are publicly available at the NAIF archive: https://naif.jpl.nasa.gov/pub/naif/EUROPACLIPPER/kernels/spk/.

Table 1 Europa's radii. Mean radius in km, semi-major (tidal), semi-minor, and polar radius, respectively (Nimmo et al. 2007)

Mean radius	a-axis	b-axis	c-axis
1560.8 km	1562.6 km	1560.3 km	1559.3 km

Table 2 Europa's orientation model. α_0 and δ_0 are the ICRF coordinates of Europa's north pole of rotation at epoch J2000.0 (Archinal et al. 2018). W is the location of Europa's prime meridian. T is the interval in the Julian centuries (36,525 days) from the standard epoch and d is the interval in days from the standard epoch. The standard epoch is JD 2451545.0 or Jan 1, 2000, 12 h Barycentric Dynamical Time (TDB)

$$\alpha_0 = 268.08 - 0.009T + 1.086 \sin J_4 + 0.060 \sin J_5 + 0.015 \sin J_6 + 0.009 \sin J_7$$
$$\delta_0 = 64.51 + 0.003T + 0.468 \cos J_4 + 0.026 \cos J_5 + 0.007 \cos J_6 + 0.002 \cos J_7$$
$$W = 36.022 + 101.3747235d - 0.980 \sin J_4 - 0.054 \sin J_5 - 0.014 \sin J_6 - 0.008 \sin J_7$$

where

$$J_4 = 335.80 + 1191.3T$$
$$J_5 = 119.90 + 262.1T$$
$$J_6 = 229.80 + 64.3T$$
$$J_7 = 352.25 + 2382.6T$$

cuss how these parameters will significantly enhance our understanding of Europa's interior structure and dynamics.

2 State of Knowledge

2.1 Reference Frame

Until Europa Clipper arrives at Europa and begins acquiring data, the Europa Clipper team will use International Astronomical Union (IAU) accepted values (Archinal et al. 2018) for Europa's shape and rotation. The current, IAU-accepted values for Europa's triaxial shape (Table 1) were derived by Nimmo et al. (2007) by fitting five individual limb profiles derived from Galileo images. Despite the sparsity of the limb data, the results agree to within their errors (±0.3 km) with the triaxial shapes derived from Galileo and Voyager image photogrammetric solutions by Davies et al. (1998) and then Bland et al. (2021). Europa Clipper will provide better constraints on the moon's long-wavelength shape through a combination of REASON altimetry profiles, Europa-UVS occultations, and EIS limb profiles (see Sect. 4.1).

The IAU defines Europa's orientation in space following their standard approach of providing models for three angles: the direction of its north rotation pole (right ascension α and declination δ), and the rotation angle W, defined as the eastward angle measured along Europa's equator from the IAU-specified reference direction (the intersection of the equatorial plane with the ICRF X–Y plane at J2000.0) to the prime meridian. The direction of the spin pole varies with time due to precession and nutation. The pole location is therefore given by its International Celestial Reference Frame (ICRF) coordinates at J2000.0 plus time-varying polynomial and periodic terms. The current model for Europa's spin pole direction (Table 2) has not been updated since the IAU report of Davies et al. (1980), except in that it is now (starting with the IAU report of Davies et al. 1983) given with respect to the J2000.0 epoch rather than the 1950.0 epoch. The IAU-values originate with the observations of Lieske

(1980), who calculated the orientation of Europa's orbit pole. The IAU therefore implicitly assumes that Europa's orbit pole and spin pole are aligned (zero obliquity). The model also assumes that Europa's rotation is uniform. However, it is known on theoretical grounds that neither of these assumptions are true (Comstock and Bills 2003; Bills 2005; Bills and Scott 2022). Deviation from uniform rotation results from both the motion of the spin pole, which induces a compensating change in the rotation rate, and from forced libration in response to torques from Jupiter that result from Europa's non-uniform orbital motion. Although more complete rotation models now exist (e.g., Bills and Scott 2022) the lack of an update to Europa's IAU-endorsed orientation model over the last 45 years is largely due to the lack of direct observations to constrain those models. The Europa Clipper mission will remedy this situation with EIS images that place new limits on variations in Europa's mean longitude at a number of frequencies (see Sect. 3.1).

Although the model for Europa's spin pole has not changed since before the Voyager mission, the location of the prime meridian in inertial space at J2000.0 (W_o) has undergone small but frequent updates over time. The cartographic location of Europa's prime meridian is set by the crater Cilix, which, by definition, is located at 182°W (178°E) (Davies and Katayama 1981). The current IAU-accepted value for W_o is 36.022°. The value was updated between the IAU reports of Davies et al. (1995) (which used $W_o = 35.67°$) and Seidelmann et al. (2002) without citation, but the change was presumably due to updated cartographic work during the Galileo mission. We note that Bland et al. (2021) proposed changing W_o to 36.054° based on their Voyager and Galileo image control network (a change of $<0.01\%$), but this change has not been adopted by the IAU and therefore is not currently used by the Europa Clipper team. The creation of a new global control network from EIS images will likely require further refinement of W_o to ensure that Cilix remains at the correct longitude.

A final complication is the potential for nonsynchronous rotation of Europa (Greenberg and Weidenschilling 1984; Ashkenazy et al. 2023; Hay et al. 2023), which current observational constraints limit to a rate of $<10^{-6}$ yr^{-1} (Hoppa et al. 2001; Burnett and Hayne 2021). This constraint suggests that up to $\sim 0.01°$ of rotation could have occurred in the 30 years between the end of the Galileo mission and Europa Clipper's arrival (corresponding to <300 m at the equator). If the nonsynchronous rotation is rapid, Europa Clipper may be able to detect it by looking for changes in the inertial location of landmarks on the surface between the Voyager, Galileo, and Europa Clipper missions.

2.2 Gravity Field

The Galileo flybys, which were used to determine the degree-2 gravity field of Europa (Anderson et al. 1998; Gomez Casajus et al. 2021) did not provide sufficient spatial sampling to accurately decorrelate the estimates of the polar and equatorial gravitational flattening ($J_2 = -C_{20}$ and C_{22} respectively). Given the mostly equatorial passes of Galileo, C_{22} is independently much better determined than J_2. The ratio between these two coefficients is a direct indicator of whether the body is in hydrostatic equilibrium. Considering the limited sensitivity of Galileo data to J_2, almost all gravity solutions have used a constraint to impose the hydrostatic equilibrium (i.e., unnormalized $J_2/C_{22} = 10/3$, or slightly less, see Tricarico 2014). The possible hydrostaticity of Europa's interior has profound implications for the determination and interpretation of its Moment of Inertia (MoI). If a body is in hydrostatic equilibrium, then the MoI can be derived directly from the gravity field coefficients (Radau-Darwin approximation, e.g., Murray and Dermott 2000). If this condition is not met, however, other methods must be used (Iess et al. 2014; Park et al. 2025). The non-hydrostatic approach considers uncertainties in gravity and topography, resulting in higher uncertainties

in Moment of Inertia (MoI). In contrast, the hydrostatic equilibrium method computes the MoI using the C_{22} estimate, providing a more precise understanding of internal differentiation based solely on gravity data, yet this might give rise to misinterpretation if the body is in fact non-hydrostatic (Gao and Stevenson 2013). No gravity coefficients beyond degree two have been measured to date.

2.3 Tidal Deformation

Europa's tidal deformation is described in terms of the degree-2 Love numbers k_2 and h_2, which quantify the perturbation of the external potential and the radial displacement, respectively. Although these values have not yet been measured directly, interior models predict ranges of plausible values depending on the presence and thickness of the ice shell. For models that include a global subsurface ocean overlain by a thin–moderate shell (∼0–30 km), h_2 is expected to be on the order of 1.1–1.3, with $k_2 \approx 0.24$–0.26 (Wahr et al. 2006; Moore and Schubert 2000). Thicker or mechanically stiffer shells ($\geq$ 50–100 km) yield lower responses, with h_2 decreasing to ∼0.6–1.2 and k_2 to ∼0.14–0.24 (Moore and Schubert 2000). By contrast, in the absence of a global ocean, the predicted deformation is extremely small, with $k_2 < 0.015$ and $h_2 < 0.1$, an order of magnitude below the oceanic case (Moore and Schubert 2000).

3 Relevant Datasets

3.1 Europa Imaging System

The Europa Imaging System (EIS) consists of a Narrow-Angle Camera (NAC) and a Wide-Angle Camera (WAC). As part of the planned EIS observations, two datasets are pertinent to geodesy (Turtle et al. 2024). The first of these is the limb profile dataset, which addresses the global shape and long-baseline slopes of Europa. The main dataset consists of framing mode images of the illuminated limb with a ground sample distance (GSD) between 0.4 and 1.0 km/pixel, obtained with the NAC at ranges between 40,000 and 100,000 km. The objective as specified by Europa Clipper planning guidelines is to obtain eight or more such profiles per hemisphere and a maximum longitudinal gap of 45° between the profiles. Gaps in this collection are to be filled with images having GSD $\leq$2.0 km, with a maximum longitude gap of 15° between profiles.

The second dataset is the so-called "Geodesy Campaign," designed to measure the amplitude of diurnal libration and other rotational parameters, and to form the starting point for a global geodetic control network that will define feature locations, permit construction of a global image mosaic, and facilitate the joint analysis of disparate remote sensing observations. Geodesy Campaign observations are NAC framing camera images with incidence angles between 20° and 80°, emission angles $\leq$75°, and phase angles $\leq$135°. The Europa Clipper planning guidelines specify that two complete "belts" of images, each encircling Europa at roughly constant latitude are to be obtained, one consisting of images obtained at true anomalies close to 90° and the other at true anomalies close to 270° (where the two extremes of diurnal libration occur). These belts are to be obtained at the same latitude and to overlap. For each, the main dataset consists of images with a GSD between 0.01 and 0.05 km/pixel taken within ±30° of the intended true anomaly. Two additional sets of guidelines define additional images to fill gaps in the main observations. True anomaly gap fill images have a GSD in the same range but a true anomaly within ±90° of the optimum, and pixel scale

fill images have a true anomaly in the $\pm 30°$ range but a GSD $\leq$0.3 km/pixel. As we discuss in Sect. 4.2, illumination conditions make it impossible to obtain 360° longitude coverage in both true anomaly ranges during the prime mission, but the scientific and cartographic objectives are not compromised if only one of the belts is gap-free.

We also note that a key goal of EIS is to produce a global controlled image mosaic covering $\geq$80% of Europa's surface at $\leq$100-m spatial scale. This will be achieved by collecting a global set of NAC framing images with GSD $\leq$100 m and performing a photogrammetric bundle adjustment to generate a geodetic control network on which the controlled mosaic will be based. The Geodesy Campaign belts will provide both an estimate of the diurnal libration and a precise longitudinal reference system on which the global network will be based. The global network, in turn, will reduce the latitudinal errors to which the narrow Geodesy Campaign belts are subject.

3.2 Gravity/Radio Science Investigation

The Gravity/Radio Science dataset is based on radiometric tracking of Europa Clipper, acquired from the NASA Deep Space Network (DSN) ground stations (Mazarico et al. 2023). These antennas transmit a highly stable uplink signal to the probe, which hosts an onboard deep space transponder that locks onto the signal and coherently retransmits it back at a slightly higher downlink frequency, enabling a two-way X/X or X/Ka configuration. Extremely accurate and stable clocks at the DSN station allow for the precise comparison of the transmitted and received frequencies, yielding highly accurate Doppler (also called range-rate) measurements. The Doppler frequency shift measures the relative velocity in the line-of-sight between the spacecraft and the DSN antenna. These observations provide constraints on the spacecraft dynamics around Europa and indirect information on the perturbing forces, including gravitational effects. Because Europa Clipper maintains nadir pointing during the flybys, the low-gain and fan-beam antennas will be used to enable telecommunication with the DSN antennas. No single antenna can remain visible and with sufficient link to the DSN stations during the whole ground track and allow radio tracking. Thus, the most favorable link margins are selected in sequence, with typically 2-3 antenna swaps needed per flyby and only short data gaps expected during switching. However, the signal-to-noise ratio (SNR) is still limited which can impact the quality of the Doppler data. To carry out Europa Clipper tracking at these low signal-to-noise ratio regimes, open-loop receivers at the DSN station will leverage post-processing methods to better capture the carrier (Buccino et al. 2023, 2024).

The determination of the static and time-variable gravity field of Europa is the primary contribution of G/RS to geodetic investigations. This is accomplished through precise orbit determination (POD) methodologies, which have demonstrated remarkable achievements in characterizing mass anomalies and distributions within celestial bodies across the Solar System. In brief, the spacecraft trajectory is time-integrated using models of physical forces, including gravity, to determine predictions of the Doppler measurements at a given acquisition time. A comparison between these model-based data with acquired Doppler observations leads to the computation of discrepancies that are minimized through an iterative process by retrieving estimates and formal uncertainties of parameters associated with force or measurement models. This method enables the estimation of all physical and observational effects producing a Doppler effect larger than the tracking system noise floor (0.05-0.1 mm/s at 60-s integration time, Mazarico et al. 2023). Considering the planned Europa Clipper flyby tour and the expected G/RS investigation performance, key physical parameters of Europa will be determined to much better accuracy than current knowledge (Sects. 4.3 and 4.4).

In addition to constraining the spacecraft trajectory and Europa's gravity parameters, the radio signals between the DSN stations and the spacecraft also enable two-way radio occultation experiments to be conducted when geometry allows. As the spacecraft gets occulted by Europa, as seen from the Earth, the frequency shift of the signal, sensitive to the refractive index of the media crossed, is used to yield information on the ionosphere (notably the electron density) in the immediate surroundings of Europa. The timing of these occultations may also be used to constrain the radius of Europa at the specific location where the ray gets blocked. This technique was particularly important at Mercury to provide absolute shape information in the southern hemisphere and support image-based shape determination (Perry et al. 2015). In concert with Europa-UVS occultations (Sect. 3.4), these observations may provide complementary information to EIS (Sect. 3.1) and REASON (Sect. 3.3) data for the determination of Europa's global shape (Sect. 4.1).

3.3 REASON Altimetry

While being primarily designed as a subsurface sounder, the 60 MHz VHF band of REASON will be used to acquire altimetric measurements during flybys of Europa at altitudes below 1000 km (Blankenship et al. 2024). The vertical resolution of the altimetry can reach 15 m; however, a lower accuracy can be expected given the ambiguity of the location of the radar returns if not discriminated by interferometry (Steinbrügge et al. 2022). A better vertical resolution and higher accuracy can be obtained by combining radargrams with cluttergrams derived from topographic information. This method will be applied when EIS stereo images, typically from the WAC, are available and allows to cross-correlate the topography derived cluttergrams with the radargrams collected by the VHF channel. Determining the offset of two radargrams above a ground-track intersection results in a measurement of the differential offset to within a few meters (Steinbrügge et al. 2018). This method is informally called "ranging" to distinguish it from the lower accuracy radar altimetry and should not be confused with the ranging technique commonly used by radio science experiments.

3.4 Europa-UVS Stellar Occultations

The Europa-UVS instrument was primarily designed to study the atmosphere and surface composition of Europa. One of the most powerful methods to study the atmosphere is through stellar occultations, when absorption of starlight as a function of wavelength and depth into the atmosphere will be used to measure its composition and vertical structure as stars appear to pass behind Europa as viewed from Europa Clipper. The atmosphere of Europa is quite tenuous and will only absorb a moderate percentage of starlight even at the greatest depths probed by stellar occultations. Thus, for each occultation, a precise measurement of the radial distance of the surface at the egress or ingress point can be captured when the remaining light from the star completely disappears. The high temporal resolution (1 ms) offered by Europa-UVS corresponds to a topographic precision on the order of meters. Abrahams et al. (2021) found that capitalizing on this precision and the already planned stellar occultation dataset that consists of > 100 events, in concert with the expected REASON radar dataset, offers further constraints to the measured topography of Europa of up to five extra spherical harmonic degrees beyond the REASON dataset used alone. In addition, the number of planned occultations is roughly one-fifth of the total number of possible occultations by Europa that Europa-UVS could observe during the mission. Europa Clipper could capitalize on these additional occultation opportunities as data volume and downlink allow.

4 Geodetic Investigations

4.1 Global Shape and Topography

The recovery of Europa's shape, or equivalently, the long-wavelength topography of Europa is desirable for several reasons. First, it can be used in combination with radar sounding to test whether the ice shell is in isostatic equilibrium. Second, when used jointly with gravity measurements, it can be employed to infer not only the mean ice shell thickness and compensation state but also spatial variations in shell thickness. Such an approach has already proven effective at Enceladus, where combining shape and gravity data enabled the mapping of hemispheric-scale shell thickness variations, revealing a thinned shell beneath the south polar terrain (Hemingway and Mittal 2019). Applying similar techniques at Europa would allow investigation of whether lateral variations in shell thickness exist, potentially linked to patterns of tidal heating, ocean dynamics, or regional geologic activity. Third, it provides a constraint that can be applied to shorter-wavelength topographic data sets (e.g., stereo topography). Information about the long spatial-wavelength topography will come primarily from EIS limb images and REASON altimetry, both of which yield profiles, and point measurements from Europa-UVS stellar occultations. Although EIS stereo observations, are a primary source of information about *local* topography, they contribute little to the recovery of the global shape because of their restricted coverage and poorer absolute accuracy. In this section, we describe the expected magnitude of long-wavelength topography (or slopes) to be measured, the expected accuracy of topographic measurements, and the limitations that arise when the various elevation measurements are combined into a global shape model by fitting a spherical harmonic expansion.

For definiteness, we estimate the RMS slope over baselines of 1225 km. This is half the 2450-km wavelength of the spherical harmonics of degree 4, which is an arbitrary but reasonable cutoff between "topography" and Europa's overall ellipsoidal shape. Galileo Solid State Imager (SSI) limb images provide information about the amplitude of topography on Europa over somewhat shorter distances. Nimmo et al. (2011) plotted the power-spectral density of limb topography for wavenumbers between 0.001 and 1 km^{-1} (i.e., wavelengths 1 to 1000 km). We extrapolate their data by fitting a simple power-law (fractal) relation between topographic power and wavenumber with a slope of -1.2 (Turcotte 1993; Shepard et al. 2001). This implies that slope varies with the -0.9 power of the baseline, and the predicted slope over 1225 km is 0.011°. Slopes over shorter baselines will be greater (Steinbrügge et al. 2020) and correspondingly easier to measure.

To generate a limb profile, the location of the local edge of the illuminated disk must be identified (Dermott and Thomas 1988). This is typically done by scanning across a pixel row or column and looking for where the digital-number (DN, i.e. brightness) value approaches within some fraction of the background (off-disk) value. Our approach will follow that used by New Horizons at Pluto and documented in Nimmo et al. (2017). Comparison of this approach with that of Thomas (2010) for Rhea images shows a median difference in limb location of 0.13-0.25 pixels. A key question about the design of the EIS limb investigation is what GSDs in the range defined by the planning guidelines are most valuable and thus at what ranges images should be obtained. The precision of the slope estimate is clearly optimized at small GSD. If a point on the limb can be located with a relative precision of r pixels, the precision in km is $r\ GSD$. The slope over a multi-pixel baseline can then be estimated by linear regression of the form $y = ax + b$, where x is the along-limb coordinate, y is the location of the limb measured perpendicular to its extent, and a is the desired slope

estimate. If N_p points are measured, the formal uncertainties of the regression parameters are then (Neter et al. 1985)

$$\begin{aligned} \sigma_a &= \rho GSD/\sqrt{S_{xx}} \\ \sigma_b &= \rho \frac{GSD}{\sqrt{N_p}} \quad . \end{aligned} \tag{1}$$

For a uniform distribution of points over an interval L (i.e., every pixel along a stretch of limb) the sum of squares is approximately $S_{xx} = N_p L^2/12$, so

$$\sigma_a = \frac{\rho GSD/\sqrt{N_p}}{L/(2\sqrt{3})} \quad . \tag{2}$$

If we measure every pixel along the limb, $N_p = L/GSD$, so both s_a and s_b are proportional to $GSD^{3/2}$, suggesting GSD should be as small as possible. The counterargument is that if multiple images are needed to span the disk, the small registration errors between frames will distort topographic profile. For example, at 0.4 km/pixel, at least 3 frames would be needed to span the diameter of Europa if the long axis of the rectangular NAC framing area is oriented north-south (so the images adjoin on their short sides), and 5 frames if the long axis is east-west. We consider a linear chain of images (i.e., neglecting the curvature of the limb) and investigate both camera orientations as limiting cases, though the actual spacecraft pointing is planned to be closer to the former. We assume the images in this chain are controlled by bundle adjustment and evaluate the post-adjustment residual errors. Note that the images will not actually be mosaicked based on the adjustment, because this would require resampling that would degrade the resolution. Instead, profile segments will be measured in each frame and combined based on the adjusted alignment between the images.

At each seam (the boundary or overlap region where two adjacent frames in an image chain meet), there will be both an offset and a rotation between successive images in the chain relative to perfect alignment. For small rotations, the problem reduces to a linear regression of cross-seam coordinates against along-seam tiepoints positions, so the uncertainties in translation and rotation are given by σ_b and σ_a calculated according to the above equations. The number of tiepoints N_p is determined by assuming they are spaced every 100 pixels along the seam, a density that is readily achievable with contemporary image-matching algorithms (Garcia et al. 2015; Bland et al. 2021). We also consider a scenario in which an additional image is centered on each seam in the primary sequence, which substantially reduces the per-seam errors. In this case, we assume a two-dimensional array of tiepoints spaced every 100 lines and samples. We assume a matching precision of $r = 0.1$ pixel for seam tiepoints, based on the lack of complicating factors such as illumination changes or stereo parallax. We also assume 0.1 pixel for limb locations (Thomas et al. 1998), though as noted above, the inconsistency between different algorithms suggests the errors could be larger. These estimates exclude the error contributed by small variations in camera pointing ("jitter") over the time needed to read out the successive lines of an EIS frame image. Such jitter distortions could be on the order of a NAC pixel, but Kirk et al. (2018) demonstrated that the errors can be reduced to less than 0.1 pixel by reading out some image lines more than once and using them as "check lines" to model the jitter.

The error propagation from individual seams to the full chain of images and hence to slope estimates over a given baseline is complicated, so we performed a series of Monte Carlo simulations based on random offset and rotation errors at each seam with the statistics just described. The calculation also assumes that any net rotation across the entire limb will

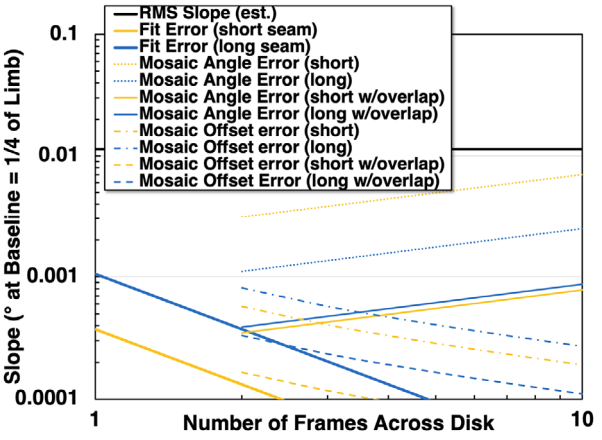

Fig. 2 Comparison of slope-measurement precision and accumulated errors in a multi-image limb observation with expected long-wavelength slopes on Europa. Because the EIS framing area is rectangular, the image GSD will be different for the same number of frames spanning the disk in the "short seam" (long axis of frame north-south) and "long seam" cases. The spacecraft orientation is expected to be closer to the short seam case. Including extra (overlap) frames at each seam substantially reduces the angle errors

be removed before slopes over the baseline of interest are calculated. The results, which are presented in Fig. 2, show the expected scaling with the number of frames (and implicitly with its inverse, the image GSD). Like the slope measurement errors, the accumulated seam offsets are smaller for small GSD (more images), but the effect of rotations propagates across the whole mosaic, so errors increase as more images are used. When added together, the total error stays well below the expected slope signal (0.011°) as long as overlap images are included. Without overlap, rotation errors grow with the number of seams and can reach about one tenth of the signal. Because EIS mosaics will include overlap and will be acquired as two-dimensional image sequences, the actual total error should remain comfortably below the signal. The EIS team therefore plans to collect these extra images. The rotational errors will also be reduced relative to the results shown because the image sequence will be a two-dimensional mosaic covering the illuminated disk, rather than a single row of images as assumed. Finally, combining an array of images with smaller GSD and a single frame covering the whole limb from farther away is another option to reduce the registration errors.

The second contribution to the long-wavelength topography will come from REASON which will be collected at altitudes below 1000 km. Given the nature of the flyby trajectory, these altimetry profiles are mostly covering the sub-jovian and anti-jovian panels (Blankenship et al. 2024). At regional and hemispherical scales, altimetry measurements can be used to test for isostasy. The range will be measured by fitting the radar return to the idealized waveform of the radar echoes as the first return is typically not the nadir return. Instead, the part of the waveform picked by fitting the waveform is most likely the range to the first large, flat portion of the surface within the radar footprint. Using comparable SHARAD sounder data on Mars it was shown that valid altimetry profiles can be derived using this technique (Steinbrügge et al. 2022). While the resolution of the VHF antenna in vacuum is 15 m, surface clutter and the high surface roughness of Europa (Steinbrügge et al. 2020) at the footprint scale likely degrade the accuracy of the altimetry which is expected to be on the order of 10s of meters.

To increase the coverage, REASON and EIS data can be combined with point measurements of chord length from UV occultations (Retherford et al. 2024). The chord is the distance between the two points where that line of sight enters and exits at that tangent height. Because the temporal resolution of Europa-UVS can be as short as 1 ms, the potential precision of the chord length measurement is $\sim$1 m, much higher than that of either EIS or REASON. However, the main advantage of UV measurements is that they fill in gaps in EIS

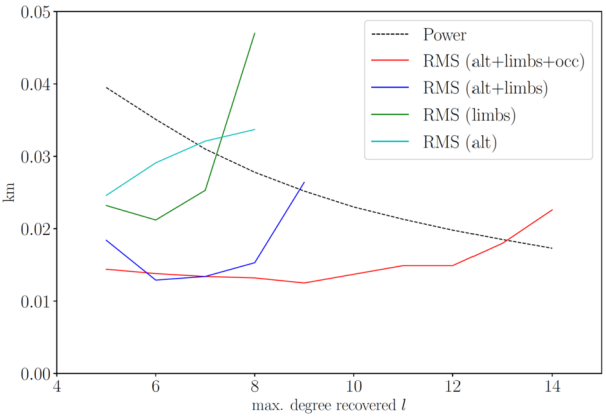

Fig. 3 Comparison of RMS misfit in recovered topography compared with topographic power at that spherical harmonic degree. The maximum degree recovered is where the solid lines intersect the dashed line. Note the large improvement when occultation measurements are added in. "Alt" = REASON altimetry and "occ" = Europa-UVS occultations

and REASON coverage centered on the leading and trailing hemispheres (Abrahams et al. 2021). Such gaps are important as they limit our ability to recover global spherical harmonic topography coefficients (Nimmo et al. 2011).

Figure 3 demonstrates how the recovery of global topography depends on which data sets are used. These results are based on synthetic data generated from a nominal shape model resolved to spherical harmonic degree and order 180, which includes contributions from hydrostatic degree-two and degree-four components, long-wavelength variations associated with tidal heating, and randomized higher-degree topography following the power spectrum derived from Galileo limb profiles (Koh et al. 2022). Occultations are incorporated into the global shape inversion as synthetic chord-length measurements, solved in a least-squares framework alongside radar altimetry and limb data. The maximum spherical harmonic degree recovered is determined when the RMS misfit (solid lines) exceeds the power in the topography (dashed line). Thus, for instance, using limb profiles alone the maximum spherical harmonic degree that can be recovered is $l = 7$. Combining limb profiles and altimetry increases the maximum degree to $l = 9$. Adding in the occultation data set results in a marked improvement, to $l = 13$ ($\sim$750 km wavelength), because these measurements fill in the EIS/REASON coverage gaps.

In general, loss of one or two flyby passes has no significant impact on the topography recovered. Two exceptions, however, are flybys E1 and E2. In the absence of occultation data, loss of limb profiles from both of these flybys would significantly widen the gaps at the leading and trailing hemispheres and reduce the maximum spherical harmonic degree recovered by 4. Another important factor is the maximum range at which REASON altimetry can be derived. In the absence of other data, reducing the maximum range from 1000 km to 500 km reduces the maximum l recovered by 4-6 (see also Abrahams et al. 2021). Inclusion of occultation chords always increases the maximum l recovered.

4.2 Rotational State and Positional Geodesy

The primary approach to understanding Europa's rotation, needed both for mapping and as a potential constraint on geophysical modeling, is the construction of a global geodetic control network from overlapping images. Once corresponding features have been measured in the image overlaps and any additional constraints such as elevations from a global shape model are available, photogrammetric bundle adjustment can be performed (e.g., Bland et al. 2018). This is a simultaneous least-squares estimation process for the ground coordinates of

the features and improved camera pointing and/or position data for the images. Rotational parameters such as the amplitude of diurnal libration can also be solved for as part of the adjustment (e.g., Oberst et al. 2014). The images constituting the global image mosaic would be included in the adjustment, but the "backbone" of the global control network will be the images from the geodesy dataset, which are optimized for estimation of the diurnal libration and obliquity. Properly estimating the precision with which these parameters can be recovered would require simulating the entire network, but simple scaling arguments give a rough idea of the precision that can be expected.

As described in Sect. 3.1, the EIS geodesy dataset consists of a set of 10- to 50-m/pixel NAC framing mode images corrected for internal jitter distortions (Kirk et al. 2016) along a "belt" that encircles Europa at low latitude. Roughly 600 images would be needed to span the full longitude range at 10 m/pixel. EIS planning guidelines specify acquiring two independent (but overlapping) belts near the extremes of the diurnal libration (true anomalies TA = 90° and 270°) but this is not achievable during the prime mission. The TA 270° belt can be closed with images taken at ≥80% of maximum libration, but longitudes 280° to 310°E remain unilluminated when the TA is near 90°. The slow rotation of the Sun-Jupiter line with respect to Europa's orbit will eventually make it possible to image this area. Encounters E50-E53, which are included in the current tour design but not the prime mission, would reduce the gap from about 40° to around 7°, and a few additional encounters might close it entirely. In any case, as discussed in more detail below, it is not essential that both belts be complete, either as the basis for controlled map products or for estimating rotational parameters.

We used Monte Carlo simulations similar to those described in Sect. 4.1 to estimate the accumulated errors in both open and closed chains of images, which is the expected internal precision relevant to cartography. The geodesy images are acquired with the long axis of the framing area aligned north-south, corresponding to "long seams." We assume a matching precision r = 0.2 pixel (e.g., Kirk et al. 2016), worse than the 0.1 pixel precision assumed for limb images, because the geodesy images will have nonidentical illumination and viewing geometries. With tiepoints every 100 pixels, this results in a standard error of ∼0.03 pixel (in both latitude and longitude) and a rotation error of 0.0015° between adjacent images. The simulations show that the offsets between 10 m/pixel images lead to an RMS maximum error between the ends of an open belt of ∼7 m, but the maximum error within a closed belt is only 3.5 m. Bending of the belt caused by rotational mismatches results in north-south displacements of as much as 1 km (closed) to 3 km (open). Having one belt closed suffices to achieve the smaller internal errors; the open belt is effectively controlled to it. The large bending errors could be reduced by adding images to overlap seams or to broaden the belt; embedding the geodesy image belt in a global control network (as is planned) will effectively do the latter, reducing north-south errors to a level comparable to the east-west offsets. Figure 4a shows how these results are affected by using images with larger GSD (up to 50 m/pixel in the primary dataset and up to 300 m/pixel as fill). Accumulated offset errors increase with GSD, but bending errors decrease.

Estimating the libration amplitude rests instead on comparing the *absolute* positioning of images at different orbital phases by measuring large numbers of tiepoints between the two belts. The absolute pointing knowledge for the NAC camera is 117 pixels (1σ) so the accuracy for measurements averaged over 600 images (the approximate number per belt if GSD = 10 m / pixel) is ∼ 4.7 pixels (Eq. 1). Comparing two such image sets thus has a precision $\sqrt{2}$ larger, or 6.6 pixels, regardless of whether the sets close in longitude or not. The precision of image-to-image ties is subpixel and thus contributes negligibly to the overall error. Given that most images can be obtained close to the extremes of libration, the longitudinal shift could be measured with a precision of 66 m for 10 m/pixel images and

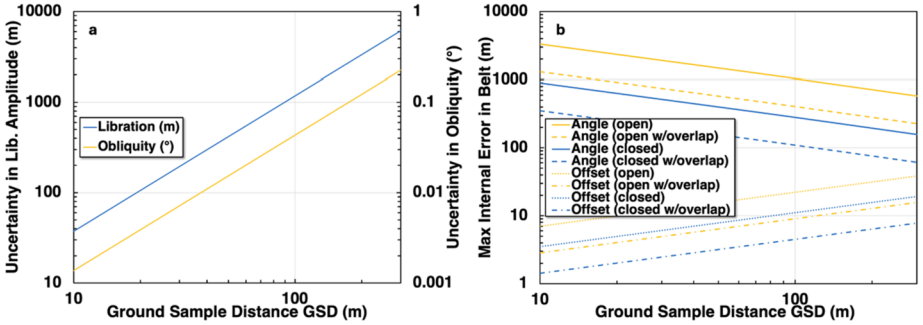

Fig. 4 (a) Errors relevant to the absolute accuracy of measurement of rotational parameters. Libration error reflects the acquisition of images at the extremes of libratory motion. Obliquity error is a lower limit assuming the pole is inclined toward one of these points on the orbit; inclination in a different direction would be less accurately estimated. (b) Errors in the "Geodesy Campaign" Europa-circling belts of images relevant to the internal precision of controlled cartographic products, as a function of the GSD and hence the number of images in a belt. Offsets affect both north-south and east-west errors; angular misalignment of images leads to larger errors in the north-south direction only. These bending errors will be reduced by embedding the belt in a global set of images with larger GSD. Errors in a closed belt are half those in a belt with a longitudinal gap, but an open belt tied to a closed one will benefit from its lower errors

the amplitude could be measured with a 1 σ uncertainty of 33 m. This compares with the expected libration amplitude of ~150 m (Van Hoolst et al. 2013). As shown in Fig. 4b, the error increases as the 3/2 power of GSD because of the increased pixel size and decreased number of images averaged. The precision of estimation for the obliquity is similar because obliquity also leads to an (apparent) variation in the location of surface features at the orbital period. The differences are 1) that at low latitudes the motions are primarily north-south rather than east-west, and 2) the true anomaly at which the excursions are greatest depends on the right ascension of the spin pole. If the images sampled the optimal orbital phases, the motion could be measured to 66 m and the pole position to 33 m, equivalent to 0.0012° in declination. This may be compared with the expected obliquity of ~0.05° (Chen et al. 2014). As for libration, the error scales as $GSD^{3/2}$.

A similar argument yields a rough estimate of the precision with which departures from synchronous rotation can be estimated. For a linear regression analysis of 600 apparent offsets spanning the ~four-year duration of the mission, the 1 σ uncertainty in the time derivative would be $6\text{x}10^{-6}$ degrees per day. This may be compared with a precision of $\sim 10^{-5}$ degree per day needed to avoid aliasing of the degree-two gravitational field components (Mazarico et al. 2023). The apparent displacement caused by longer period librations could potentially be measured at a similar level of precision, but if the Europa Clipper mission lasts only a fraction of a libration period, then the amplitude would be less well determined. In particular, it will not be possible to distinguish librations sampled over only a small fraction of a cycle from one another or from a purely secular nonsynchronous rotation rate. An alternative approach to estimating nonsynchronous rotation would be to compare the distance between local features and the terminator with those observed for the same features by Galileo or Voyager. This provides a much longer time baseline, but the achievable precision is limited by the precision with which the terminator itself can be localized and does not benefit from the higher resolution achievable with EIS. EIS images or mosaics extending from the limb to the center of the disk (e.g., those obtained for limb profiling with phase angles $\leq$90°) could also potentially be used to locate features with respect to the limb, and thus the sub-spacecraft point, but the pre-Clipper observations relied on terminator images.

Hoppa et al. (1999) found that the primary error source was the influence of local-scale topography on the terminator position and estimated a localization precision of 0.3° (8 km). It remains to be determined whether this precision could be improved by topographic mapping using EIS stereo pairs. If not, the rotational precision for terminator measurements would be several times 10^{-5} degrees per day.

Finally, the rotational parameter W_0 describes the orientation of Europa's prime meridian in inertial space at the reference time J2000.0. This parameter has no geophysical significance but is essential for cartography because it defines the prime meridian and the longitude of all other features. Europa's longitude system is defined such that the crater Cilix has a longitude of 182°W (Archinal et al. 2018), so W_0 derives uncertainty from both the absolute accuracy of the EIS position and pointing and the internal precision of the control network that connects the images to Cilix. To keep the crater at its defined longitude, W_0 must thus be updated every time the control network is recalculated. It is likely that such control calculations will be performed multiple times during the mission as data are acquired (at a minimum, after the conclusion of Europa Campaigns 1 and 2), yielding updated values of W_0, obliquity, rotation rate, and libration amplitude—as well as spatial referencing of the images—that will be used within the Europa Clipper mission for subsequent observation planning and cartographic product generation. Documentation of the final estimates of these parameters in the peer-reviewed literature would make it possible for the International Astronomical Union Working Group on Cartographic Coordinates and Rotational Elements of the Planets and Satellites to recommend adoption of the best post-mission values by the research community.

Further, the determination of the degree-2 gravity coefficients enables the refinement of the orientation of the body principal axes. In terms of spherical harmonics, the gravity field defines the principal axes as the reference frame that satisfies $C_{21} = S_{21} = S_{22} = 0$. Previous solutions have not imposed this constraint and instead estimated these coefficients (see Table 3). Although consistent within 3σ, the solutions from Anderson et al. (1998), Jacobson et al. (2000) and Gomez Casajus et al. (2021) show different angular values for the principal axes in the conventional Europa body fixed frame (the IAU-defined body frame; Archinal et al. 2018), as shown in Fig. 5. The reduced uncertainty on the degree-2 gravity that Europa Clipper will enable a substantial improvement in the orientation of Europa's principal axes. This will allow reducing the uncertainty in the transformation between principal axes and cartographic axes, thus reducing the error propagation for those products that need to be mapped from one frame to the other.

4.3 Static Gravity Field (G/RS)

The G/RS experiment onboard Europa Clipper will measure the gravity field of Europa by means of radiometric Doppler tracking (see Sect. 3.2). The precise reconstruction of the spacecraft trajectory enables the estimation of Europa's static gravity field, including the point-mass effect and deviations associated with the heterogeneous mass distribution, and of its time-variable gravitational response to the changing gravitational effect of external bodies (mainly Jupiter, see Sect. 4.4). The gravitational potential of a body is typically represented as a series expansion of spherical harmonics functions (e.g., Kaula 2000), whose degree of expansion (l) corresponds to the minimum resolved wavelength (λ). In the case of Europa Clipper, the maximum resolvable degree is predicted to be between $l = 8$ and $l = 15$ (corresponding to wavelength $\lambda = 615 - 330$ km, defined as $\lambda = \pi R / l$.), depending on the actual strength of the field, which is not currently known. A detailed description of the expected measurement performance of G/RS can be found in Mazarico et al. (2023).

Table 3 Values and Uncertainties for Key Geophysical Parameters

Parameter	Current value	Current uncertainty	Uncertainty after Europa Clipper
C20	435×10^{-6} [1] 461×10^{-6} [2]	8×10^{-5} [1,2]	$3.5 - 8.5 \times 10^{-7}$
C21	-1.4×10^{-6} [1] 4.2×10^{-6} [2]	6.0×10^{-6} [1] 11.7×10^{-6} [2]	$4 - 9 \times 10^{-7}$
C22	131×10^{-6} [1] -139×10^{-6} [2]	2.5×10^{-6} [1,2]	$1.5 - 2.3 \times 10^{-7}$
S21	14×10^{-6} [1] 7.4×10^{-6} [2]	12×10^{-6} [1] 10×10^{-6} [2]	$3 - 8 \times 10^{-7}$
S22	-13×10^{-6} [1] -6.7×10^{-6} [2]	29×10^{-6} [1] 25×10^{-6} [2]	$6 - 9 \times 10^{-7}$
Max spherical harmonic degree gravity field	2	-	8-15
Max spherical harmonic degree shape	2	-	9-14
k_2	-	-	0.015
h_2	-	-	0.06
Libration amplitude	-	-	1.2×10^{-3} deg
Pole right ascension	268.08 deg	0.27×10^{-7} [3]	0.08 - 0.20 deg
Pole declination	64.51 deg	0.07×10^{-7} [3]	0.04 - 0.08 deg (G/RS) 0.0012 (EIS)
Obliquity	0.1 - 1.5 deg [4,5] (indirect)	-	0.04 - 0.08 deg

Notes: The spin rate was not estimated as it may be more accurately determined from EIS imagery. References [1] Jacobson et al. (2000), [2] Gomez Casajus et al. (2021) [3] Davies and Katayama (1981) [4] Bills et al. (2009) [5] Rhoden et al. (2010). Table adapted from Mazarico et al. (2023).

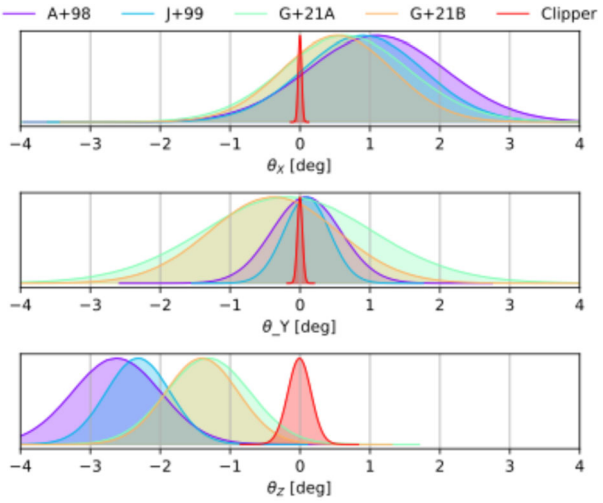

Fig. 5 Comparison of the determination of the Principal Axes in the IAU reference frame, between previous solutions (A+98: Anderson et al. 1998; J+99 Jacobson et al. 2000; G+21A and B Gomez Casajus et al. 2021 solutions A and B) and the expected Europa Clipper results. The three panels show the distribution of the three rotation angles. Note that a central value of zero is assumed here for the Europa Clipper case, while the measured values of the C_{21}, S_{21}, S_{22} coefficients are used for the published solutions

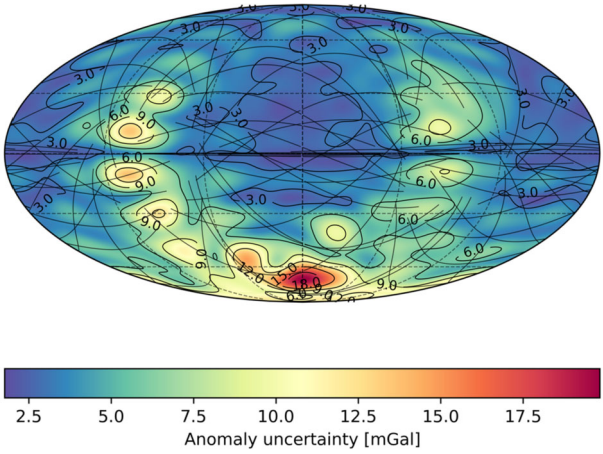

Fig. 6 Europa gravity anomaly uncertainty that will be retrieved by Europa Clipper. The gravity field is expanded up to spherical harmonic degree 10, and the uncertainties are obtained from numerical simulations conducted on the trajectory 21F31V5. Groundtracks below 3000 km altitude are shown as black lines. The map is in a Mollweide projection centered on longitude 180°E

Here, we focus instead on the geodetic implications of the anticipated G/RS measurements, namely we discuss the expected capability of Europa Clipper to determine whether Europa is in hydrostatic equilibrium, the retrieved uncertainty on the gravity anomaly, the capability of separating the deep interior and the icy shell contributions to the gravity field.

Unlike Galileo, Europa Clipper, with its numerous flybys with varying geometry, will enable an independent estimation of J_2 and C_{22} leading to an uncertainty on their ratio of 0.003 and a correlation of 0.03, which is important to determine whether Europa is in hydrostatic equilibrium (Sect. 3.2).

At long wavelengths (low spherical harmonic degrees, $l < 30$), Europa's gravity field is expected to be dominated by the silicate deep interior (e.g., Pauer et al. 2010; Koh et al. 2022; Cascioli et al. 2024). This is due to the intrinsic mechanical weakness of the icy shell, which is expected to be fully compensated at long wavelengths. The measured global gravity field will thus mainly provide information on the silicate interior of Europa, and a unique opportunity to study it. Previous analyses have shown that the global gravity field may provide constraints on the deep interior and seafloor properties of Europa (Cascioli et al. 2024) and thus provide fundamental information for determining the heat flow coming out of the silicate core, possibly discerning between solely radiogenic heating or additional tidal contribution, ultimately providing fundamental clues for habitability (Dombard and Sessa 2019).

Although not resolved globally, Europa Clipper G/RS data will still be sensitive to local small-scale features, thanks to the many low-altitude flybys (15% of the flybys have a closest approach distance below 30 km). This is illustrated by the global map of the uncertainty on the measured geoid (Fig. 6), showing a substantial dichotomy between sub- and anti-jovian areas (0° and 180° in longitude) where the majority of flybys will take place and the trailing and leading edges (90° and 270° lon). Gaps in the global dataset constrain the highest spherical-harmonic degree that can be reliably estimated. However, the data from the lowest-altitude flybys can be used to perform localized analyses. As demonstrated in previous studies (Goossens et al. 2022; McKenzie and Nimmo 1997), residual line-of-sight (LOS) Doppler accelerations can be used to increase local resolution and investigate the mechanical properties of the outermost regions of the body. This technique allows separation of the contributions of the deep interior (sensed through the low-degree global gravity field) and the icy shell (sensed through LOS), as illustrated by Fig. 7.

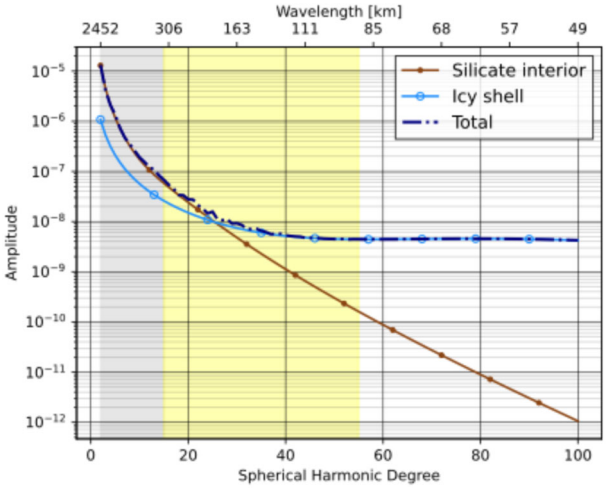

Fig. 7 Illustration of the contribution of the silicate interior and of the ice shell to the total observed gravity field of Europa, based on a simulated interior structure of the body. The deep interior dominates the signal at low spherical harmonic degree (or equivalently long wavelength). The gray shaded area shows the expected resolution range of the global gravity field solution. The yellow shaded area shows the range where the LOS technique can be expected to be sensitive (we assume here that a region of size r_{region} is resolved if at least 4 Doppler points are collected in it and the spacecraft altitude is less than r_{region}). This figure highlights how the global solution will provide sensitivity to the deep interior, while the LOS local solutions will be able to probe the characteristics of the icy shell. Figure adapted from Cascioli et al. (2024), where the details of the gravity contribution calculations are also provided

4.4 Tidal Deformation

As Europa orbits in its 1:1 spin-orbit resonance, the gravitational force exerted by Jupiter varies at the orbital period due to the Europa's orbital eccentricity and inclination. Although the tidal response depends on multiple parameters tied to a body's internal structure and rheology, it is frequently expressed in terms of tidal Love numbers—parameters that capture the net deformational effect and can be reproduced by a variety of models, including simple viscoelastic approximations.

The Love number k_2 quantifies the time-varying component (at the orbital period) of the spherical harmonic degree-2 gravity potential of Europa with respect to the input perturbing tidal potential of Jupiter. Similarly, the Love number h_2 relates the degree-2 radial surface deformation to the tidal forcing. If significant dissipation occurs (e.g., mechanical dissipation due to the periodic deformation of the ice shell), the tidal response is delayed with respect to the forcing potential (referred to as a tidal time or phase lag). To fully characterize the body's response, a comprehensive model of tidal amplitudes and phases of the Love numbers k_2 and h_2 must be accounted for in the geodetic analysis, facilitating the adjustment of these parameters through the processing of gravity and altimetry data, respectively.

A perfectly uniform and strengthless sphere would have a k_2 of 1.5 (e.g., Murray and Dermott 2000). A perfectly rigid sphere would have a k_2 of 0. Real objects will have a k_2 somewhere in between these limits. In the case of Europa, the value of k_2 is strongly dependent upon the presence of a subsurface ocean that would mechanically decouple the more deformable ice shell from the more rigid interior. Expected values are around 0.23 with an ocean and <0.015 without (Moore and Schubert 2000). As a result, the G/RS measurement accuracy objective for k_2 is 0.06, to allow distinguishing between the two cases. At every

flyby of Europa, Europa Clipper will experience a different degree-2 gravity field, according to the location of Europa in its orbit around Jupiter (true anomaly). Multiple flybys enable adequate sampling of the time-variable tidal contribution, helping to decorrelate it from the static degree-2 field. With the planned flyby tour, the k_2 accuracy requirement is expected to be met after the first 12 flybys of Europa; the nominal mission that accounts for 49 Europa flybys will enable tighter constraints on k_2 (<0.02) (Mazarico et al. 2023). This high level of accuracy of the gravitational tides, combined with complementary geophysical measurements, will confirm (or refute) the presence of an internal ocean and provide key constraints on Europa's ice shell thickness and rigidity.

This sensitivity to the ice shell thickness can be increased by measuring the amplitude of the radial deformation quantified by the tidal Love number h_2 and building the linear combination $1+k_2-h_2$ (Wahr et al. 2006). The REASON radar sounder is capable of providing such measurements by analyzing differential range data at crossover locations where two ground tracks intersect (Steinbrügge et al. 2018). Sensitivity to the tidal signal requires that these intersections sample Europa at different orbital longitudes around Jupiter, ensuring coverage across varying tidal phases. The current reference trajectory provides favorable geometry, with good spatial sampling of both sub-jovian and anti-jovian points—where the tidal bulge reaches its maximum amplitude—and sufficient temporal diversity to capture multiple true anomalies. In presence of a subsurface ocean, REASON should therefore be able to detect a maximum (double-)amplitude deformation on the order of 60 m if a global subsurface ocean is present. As this measurement depends critically on knowledge of the static topography at the crossover sites. To remove the contribution of local relief, REASON ranging will be combined with high-resolution digital terrain models from the Europa Imaging System (EIS). Stereo-derived DTMs provide the necessary constraint on local topography but introduce operational requirements: the crossover location must be illuminated during at least one of the contributing flybys, and the vertical and horizontal resolution of the DTM must be sufficient to resolve the radar footprints. When these conditions are met, the combined radar–DTM approach can achieve differential range accuracies of a few meters, enabling h_2 to be constrained with an uncertainty of ~0.04–0.17 depending on surface roughness, DTM quality, and ionospheric effects. Using a linear combination of the tidal Love numbers $1 + k_2 - h_2$, is expected to provide better constraints on the icy shell thickness compared to interior model inversions based on the analysis of k_2 and h_2 separately (Wahr et al. 2006) as the linear combination is less sensitive to the deeper interior if the ice shell is decoupled by a global ocean. However, the shell rigidity is also poorly known, introducing significant uncertainty in the determination of the ice thickness. By assuming k_2 and h_2 uncertainties of 0.015 (Mazarico et al. 2023) and 0.06 (Steinbrügge et al. 2018), respectively, the linear combination is computed with a formal uncertainty of ~0.045. Note that, the h_2 uncertainty estimate from 2018 is still valid even if the tour design evolved since then.

No appreciable phase lag is expected with typical silicate viscosities in a non-dissipative mantle (<1°, Moore and Schubert 2000). However, partial melt (e.g., Běhounková et al. 2021) would significantly lower the effective viscosity and yield up to several degrees of phase lag. The h_2 phase lag would be smaller than the k_2 phase lag if dissipation occurs in the silicate layers, so a phase lag difference between k_2 and h_2 would indicate dissipation in the deep interior (Hussmann et al. 2016).

4.5 Ephemeris

The Europa Clipper mission will play a crucial role in improving the current knowledge of Europa's ephemerides. During a spacecraft's flyby of a moon of a gas giant, such as Europa,

range-rate measurements extracted from the radio link described in Sect. 3.2 carry information on the spacecraft's position relative to the moon and the planet. Hence, by accurately reconstructing the trajectory throughout the entire flyby, the relative position of the moon with respect to the planet can be determined. Typical X-band observations achieve position accuracies of a few hundred meters within the orbital plane and tens of kilometers outside the plane. As a result, the evolution of the moon's ephemerides can be reconstructed. Accurate estimation of ephemerides is crucial, not only for spacecraft navigation but also to precisely reconstruct a moon's gravity field during flybys. Additionally, understanding the evolution of the ephemerides is essential for studying the tidal dissipation in both Jupiter and its moons. Indeed, these tidal effects produce a secular quadratic perturbation in the tangential direction of the moons' orbits and are responsible for the change in orbital energy of the system (Murray and Dermott 2000). Moreover, Europa's orbit, along with those of Io and Ganymede, is locked in the Laplace resonance. This dynamical state plays a key role in sustaining the tidal dissipation and heat production within the interiors of these moons (Malhotra 1991). The potential habitability of the moons is determined by tracing the resonance's long-term evolution. If the resonance were young or short-lasting, the conditions necessary to support life to develop may not have been stable for long enough to emerge.

Secular changes in eccentricity and mean motion arise from the combined effects of resonant interactions and tidal dissipation, and the cumulative imprint of these processes is directly measurable in the orbital elements. Ground-based astrometry provides the multi-decade to century baselines necessary to establish these secular trends (Lainey et al. 2009, 2012), while spacecraft-based ephemerides add the precision needed to resolve the shorter-period components and disentangle resonance forcing from genuine tidal damping (Fayolle et al. 2023). In carrying out our numerical simulations, we considered the four hours of radio tracking centered around the closest approach (C/A) dedicated to radio science data, exploiting the antenna which provides the highest signal-to-noise ratio (SNR). Only two-way Doppler observables using X-band for both uplink and downlink, that have an SNR above 4 dB-Hz are considered, as described in Mazarico et al. (2023). In addition to the data collected around C/A, we also exploited the standard navigation tracking passes, which are scheduled to be approximately 12 to 28 hours before and after the closest approaches, also called "flyby wings". During these tracking windows, two-way Doppler and range will be generated using the high gain antenna (HGA). The Doppler noise level used in our simulations was computed using empirical models of the main noise sources (Mazarico et al. 2023). The average noise during the C/A is expected to be around 0.1 mm/s at 60 s integration time, while it is expected to improve by about a factor of 2, that is to 0.05 mm/s at 60 s, when using the HGA. For the two-way range data, a 1 m noise jitter and a systematic error of 2 m were considered.

Figure 8 shows the expected position uncertainties of Europa in the radial, tangential, and normal directions and illustrates that consideration of the navigation passes in addition to the data at C/A improves the positions by approximately an order of magnitude. While Europa Clipper will potentially provide an unprecedented estimation of Europa's tidal lag, it might not be sufficient to improve Jupiter's tidal dissipation knowledge (Magnanini et al. 2024). However, a joint analysis with JUICE radio tracking data, could potentially improve current knowledge on Jupiter's tidal dissipation, solely from radio science data (Fayolle et al. 2023; Magnanini et al. 2024).

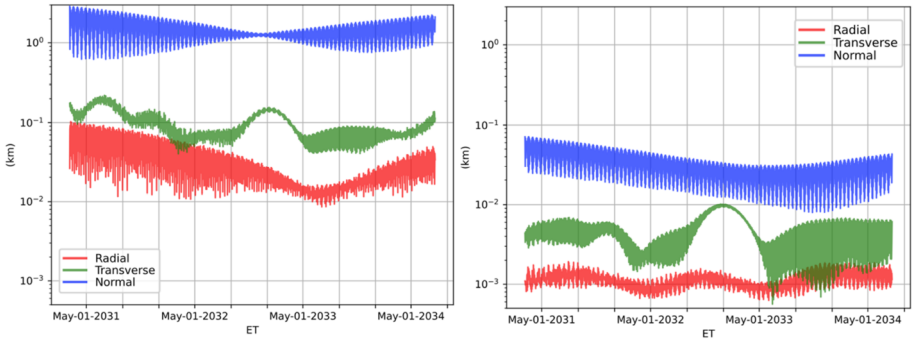

Fig. 8 Expected Europa position uncertainties (1σ) in the radial, tangential, and normal to the orbital plane directions during the Europa Clipper mission time span, with respect to the Jupiter Barycenter. The left panel displays the solution exploiting only the 4 hours around the C/A, while in the right panel both the C/A and navigation passes are considered

5 Discussion

The geodetic investigations conducted by the Europa Clipper mission will provide critical data to improve our understanding of Europa's internal structure, rotational dynamics, and tidal deformation. Measurements of Europa's global shape, rotational parameters, and gravity field will constrain the thickness and mechanical properties of the ice shell, as well as the size and composition of the subsurface ocean. These findings will be informed by a combination of altimetry profiles from REASON, limb imaging from EIS, and Europa-UVS stellar occultations, which together will establish a high-precision cartographic reference frame, necessary for accurately linking surface and subsurface features.

Analysis of Europa's rotational state will address potential deviations from synchronous rotation and provide more precise estimates of the moon's diurnal libration and obliquity. Libration and obliquity measurements provide complementary constraints on Europa's rotational state and interior. Forced librations are highly sensitive to mechanical decoupling of the ice shell, but their amplitude is also strongly modified by tidal response: the difference between fluid and dynamic Love numbers means that a significant fraction of the tidal deformation is absorbed elastically by the shell, reducing the effective torque from Jupiter by up to $\sim$90% and suppressing the libration signal (Van Hoolst et al. 2013). Additional damping arises from gravitational and pressure torques when the shell and interior librate out of phase. In the absence of tidal suppression, a decoupled shell would produce librations of order $\sim$150 m, resolvable above Clipper's $\sim$30 m (1σ) uncertainty; in practice, tidal effects likely reduce the amplitude well below this value, so detecting any signal will critically test the shell's mechanical state. Obliquity provides a parallel constraint: a solid body predicts values an order of magnitude larger than the $\sim$0.05° expected with an ocean, since ocean–ice coupling alters the Cassini state geometry (Baland et al. 2012). At Clipper's achievable precision, these differences are measurable, and recent work shows that tidal dissipation within the shell can further drive detectable departures from the classical Cassini state, linking obliquity directly to the magnitude of internal heating (Downey and Nimmo 2025). Together, libration and obliquity thus provide rotational diagnostics of shell thickness, rigidity, and ocean–ice coupling, complementing gravity and tidal Love number measurements in joint interior models.

The G/RS investigation will refine estimates of the static degree-2 gravity coefficients, enabling a more accurate assessment of Europa's moment of inertia. This will test whether

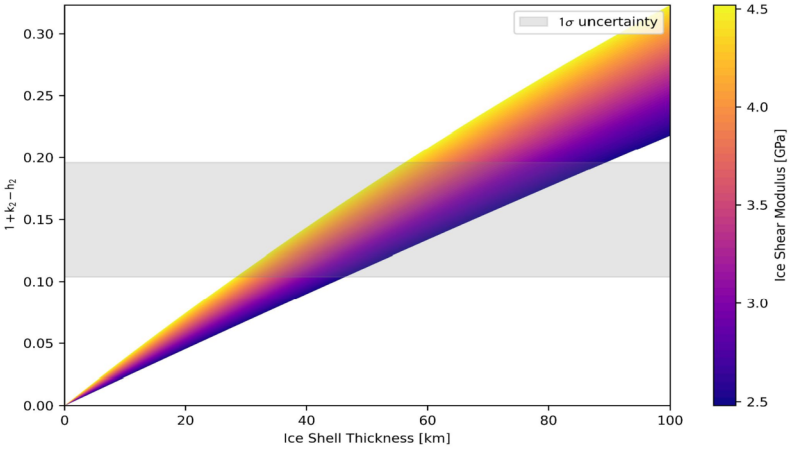

Fig. 9 Linear combination of k_2 and h_2 as a function of ice shell thickness and shear modulus. Although the sensitivity of this factor to the ocean density is significantly reduced when compared to k_2 only, significant uncertainties are introduced by the shear modulus of the icy shell. The uncertainty on the ice thickness derived from the combination of k_2 (uncertainty of 0.015; Mazarico et al. 2023) and h_2 (uncertainty of 0.06; Steinbrügge et al. 2018) is larger than 50 km. Combining the tidal Love numbers with additional measurements will be important to derive the hydrosphere structure. The models assume an ocean density of 1050 kg/m^3, hydrosphere thickness of 140 km, an elastic mantle (shear modulus of 50 GPa) with an average density of 3600 kg/m^3 overlaying a fluid core with radius 300 km and density adjusted to match the total mass. The ice shell is elastic; accounting for a viscoelastic response increases the uncertainties on the derived interior structure

the moon is in hydrostatic equilibrium and provide insights into the distribution of mass within Europa's interior.

The measurements of the tidal Love numbers (k_2 and h_2) will offer new constraints on the thickness and rheology of the ice shell, as well as on the ocean's properties, such as depth and density. Interpreted jointly, these parameters help disentangle the contributions of ice thickness, shell rheology, and ocean properties, though degeneracies remain. Figure 9 shows that an uncertainty of $\sim$2 GPa on the shear modulus significantly inflates the uncertainty on the ice shell thickness from 20 km to $>$ 50 km. Complementary geophysical data sets in a joint inversion are then key to deconvolve the ice thickness and rigidity. Magnetic induction measurements are sensitive to the radial location of Europa's conducting ocean boundaries, and under favorable conditions (ocean thickness $>$40 km and conductivity $>$1 S/m) can provide unique constraints on ice shell thickness (which would allow to break the degeneracy between ice shell thickness and rigidity), ocean thickness and conductivity with an accuracy better than $\sim$50% (Kivelson et al. 2023). A global joint inversion of geodetic and magnetic measurements will enable a comprehensive characterization of the interior structure (Petricca et al. 2023).

Improved ephemerides from Europa Clipper will also enhance our understanding of Europa's orbital evolution and tidal heating. Secular variations in eccentricity and mean motion encode the balance between resonant forcing and tidal dissipation within the Laplace resonance. Ground-based astrometry has provided the century-scale baselines needed to detect cumulative orbital drifts (Lainey et al. 2009, 2012), but spacecraft-derived ephemerides add the precision required to resolve shorter-period terms and resonance-driven variations that are otherwise inaccessible. In particular, such data can determine whether Europa's present eccentricity is sustained by resonance locking with Io and Ganymede or whether

episodes of strong damping have occurred. Distinguishing between these scenarios is essential for assessing whether Europa has experienced sustained high tidal heating over geologic timescales or intermittent cycles of ocean freezing and shell thickening. If the Europa Clipper gravity data suggest the absence of a metallic core (or presence of a small core), then this would certainly argue against episodes of intense heating due to resonance crossing. Ganymede's situation in the Laplace resonance does not necessarily imply that Europa also went through intense episodes of tidal heating. Combined with JUICE observations of Ganymede and Callisto, Europa's interior structure may then explain the extent to which the Laplace resonance drove the internal evolution of the Galilean moons.

Together, constraints from gravity, tides, rotation, and ephemerides will define the large-scale structure and long-term evolution of Europa's ice shell and ocean. To place these geophysical results into a broader planetary context, they must be coupled with compositional constraints, which address the nature of Europa's building blocks and the chemical environment of the ocean. Constraints on the bulk rock density will be used to narrow down possible sources for Europa's building blocks. Half a dozen possible models have been suggested for the origin of Europa's materials (Becker et al. 2024). Recent models based on the reanalysis of the Galileo gravity data suggest that Europa primarily accreted CV chondrites (Petricca et al. 2025). Other models have assumed ordinary chondrites as the primary building block of Europa (Kuskov and Kronrod 2005), based on early interpretations of the Galileo data. Resolving this open question will shed light on the origin of the Jovian system.

A better understanding of Europa's interior structure, coupled with compositional measurements (see Becker et al. 2024) will help unravel Europa's habitability potential. Geodetic observations combined with thermal observations (E-THEMIS) will also provide estimates of the extent of tidal heating in the icy shell with important implications for habitability (Vance et al. 2023). Evidence of topography at the surface of the rocky seafloor from static gravity would be indirect evidence for volcanic activity, at least in Europa's past, and would provide clues about Europa's thermal state. Volcanic activity might have also been involved in the replenishment of the ocean in redox species maintaining chemical gradients (see Vance et al. 2023). Those chemical gradients may help sustain a biosphere.

While inferences on the deep interior may be limited or indirect, we expect robust constraints from geodetic measurements of the dynamical response of Europa's shell. Future constraints on Europa's rotational dynamics and diurnal response to tidal forcing, combined with geology observations, will help address many open questions or revisit old problems related to Europa's orbital evolution and tidal-driven geology (see Daubar et al. 2024).

By linking interior dynamics, composition, and geological activity, Europa Clipper's geodetic data will provide an essential foundation for assessing the persistence of habitable conditions within Europa's subsurface ocean. Placed in the broader context of comparative observations by Juice, Europa Clipper's results will thus advance our understanding of how ocean worlds evolve across the Jovian system and beyond.

Funding Information A portion of this research was carried out at the Jet Propulsion Laboratory, California Institute of Technology, under a contract with the National Aeronautics and Space Administration (80NM0018D0004) and was supported by the Europa Clipper program. Work by GC was supported by NASA under award number 80GSFC24M0006. A.M., P.T., and M.Z. acknowledge financial support from the Italian Space Agency through the Agreement 2021-13-HH.1-2023. AG acknowledges funding from the Italian Space Agency (ASI) grant n. 2023-60-HH.0.

Declarations

Competing Interests The authors declare that they have no conflicts of interest.

References

Abrahams JNH, Nimmo F, Becker TM, Gladstone GR, Retherford KD, Steinbrügge G, Mazarico E (2021) Improved determination of Europa's long-wavelength topography using stellar occultations. Earth Space Sci 8:e01586. https://doi.org/10.1029/2020ea001586

Anderson JD, Schubert G, Jacobson RA, Lau EL, Moore WB, Sjogren WL (1998) Europa's differentiated internal structure: inferences from four Galileo encounters. Science 281(5385):2019–2022. https://doi.org/10.1126/science.281.5385.2019

Archinal BA, Acton CH, A'Hearn MF, Conrad A, Consolmagno GJ, Duxbury T, Hestroffer D, Hilton JL, Kirk R, Klioner SA, McCarthy D, Meech K, Oberst J, Ping J, Seidelmann PK, Tholen DJ, Thomas PC, Williams IP (2018) Report of the IAU working group on cartographic coordinates and rotational elements: 2015. Celest Mech Dyn Astron 130:22. https://doi.org/10.1007/s10569-017-9805-5

Ashkenazy Y, Tziperman E, Nimmo F (2023) Non-synchronous rotation on Europa driven by ocean currents. AGU Adv 4:e2022AV000849. https://doi.org/10.1029/2022AV000849

Baland RM, Yseboodt M, Van Hoolst T (2012) Obliquity of the Galilean satellites: the influence of a global internal liquid layer. Icarus 220(2):435–448. https://doi.org/10.1016/j.icarus.2012.05.020

Becker TM, Zolotov MY, Gudipati MS, et al (2024) Exploring the composition of Europa with the upcoming Europa Clipper Mission. Space Sci Rev 220:49. https://doi.org/10.1007/s11214-024-01069-y

Běhounková M, Tobie G, Choblet G, Kervazo M, Melwani Daswani M, Dumoulin C, Vance SD (2021) Tidally induced magmatic pulses on the Oceanic floor of Jupiter's Moon Europa. Geophys Res Lett 48:e2020GL090077. https://doi.org/10.1029/2020GL090077

Bills BG (2005) Free and forced obliquities of the Galilean satellites of Jupiter. Icarus 175:233–247. https://doi.org/10.1016/j.icarus.2004.10.028

Bills BG, Scott BR (2022) Rotation models for the Galilean satellites. Planet Space Sci 219:105474. https://doi.org/10.1016/j.pss.2022.105474

Bills BG, Nimmo F, Karatekin O, Van Hoolst T, Rambaux N, Levrard B, Laskar J (2009) Rotational dynamics of Europa. In: Pappalardo RT, McKinnon WB, Khurana KK (eds) Europa. University of Arizona Press, Tucson, pp 119–136

Bland MT, Becker TL, Edmundson KL, Roatsch T, Archinal BA, Takir D, et al (2018) A new Enceladus global control network, image mosaic, and updated pointing kernels from Cassini's 13-year mission. Earth Space Sci 5:604–621. https://doi.org/10.1029/2018EA000399

Bland MT, Weller LA, Archinal BA, Smith E, Wheeler BH (2021) Improving the usability of Galileo and Voyager images of Jupiter's Moon Europa. Earth Space Sci 8(12):e2021EA001935. https://doi.org/10.1029/2021EA001935

Blankenship DD, Moussessian A, Chapin E, et al (2024) Radar for Europa Assessment and Sounding: Ocean to Near-surface (REASON). Space Sci Rev 220:51. https://doi.org/10.1007/s11214-024-01072-3

Buccino DR, Oudrhiri K, Parisi M, Park RS, Mazarico E, Tortora P, Withers P, Genova A, Zannoni M (2023) Precision of spacecraft Doppler tracking at low signal-to-noise ratios. Radio Sci 58(7):1–8. https://doi.org/10.1029/2023RS007703

Buccino D, Parisi M, Kahan D, Yang O, Barbinis E, Oudrhiri K, Park R (2024) Precision Doppler measurements from low-SNR signals experiencing residual Doppler and acceleration. In: 2024 IEEE Aerospace Conference. IEEE, pp 1–6

Burnett ER, Hayne PO (2021) Europa's hemispheric color dichotomy as a constraint on non-synchronous rotation. Icarus 364:114438. https://doi.org/10.1016/j.icarus.2021.114438

Cascioli G, Mazarico E, Dombard AJ, Nimmo F (2024) Leveraging the gravity field spectrum for icy satellite interior structure determination: the case of Europa with the Europa Clipper Mission. Planet Sci J 5(2):45. https://doi.org/10.3847/PSJ/ad1933

Chen EMA, Nimmo F, Glatzmaier GA (2014) Tidal heating in icy satellite oceans. Icarus 229:11–30. https://doi.org/10.1016/j.icarus.2013.10.024
Comstock RL, Bills BG, (2003) A solar system survey of forced librations in longitude. Journal of Geophysical Research: Planets 108:E9. https://doi.org/10.1029/2003JE002100
Daubar IJ, Hayes AG, Collins GC, Craft KL, Rathbun JA, Spencer JR, Wyrick DY, Bland MT, Davies AG, Ernst CM, Howell SM (2024) Planned geological investigations of the Europa Clipper Mission. Space Sci Rev 220(1):18. https://doi.org/10.1007/s11214-023-01036-z
Davies ME, et al (1980) Report of the IAU working group on cartographic coordinates and rotational elements of the planets and satellites. Celest Mech 22:205–230. https://doi.org/10.1007/BF01229508
Davies ME, Katayama FY (1981) Coordinates of features on the Galilean satellites. J Geophys Res Space Phys 86:8635–8657. https://doi.org/10.1029/JA086iA10p08635
Davies ME, et al (1983) Report of the IAU working group on cartographic coordinates and rotational elements of the planets and satellites: 1982. Celest Mech 29:309–321. https://doi.org/10.1007/BF01228525
Davies ME, Abalakin VK, Bursa M, et al (1995) Report of the IAU/IAG/COSPAR working group on cartographic coordinates and rotational elements of the planets and satellites: 1994. Celest Mech Dyn Astron 63:127–148. https://doi.org/10.1007/BF00693410
Davies ME, Colvin TR, Oberst J, Zeitler W, Schuster P, Neukum G, McEwen AS, Phillips CB, Thomas PC, Veverka J, Belton MJS, Schubert G (1998) The control networks of the Galilean satellites and implications for global shape. Icarus 135(1):372–376. https://doi.org/10.1006/icar.1998.5982
Dermott SF, Thomas PC (1988) The shape and internal structure of Mimas. Icarus 73(1):25–65. https://doi.org/10.1016/0019-1035(88)90084-X
Dombard AJ, Sessa AM (2019) Gravity measurements are key in addressing the habitability of a subsurface ocean in Jupiter's Moon Europa. Icarus 325:31–38. https://doi.org/10.1016/j.icarus.2019.02.025
Downey BG, Nimmo F (2025) Titan's spin state as a constraint on tidal dissipation. Sci Adv 11(6):eadl4741. https://doi.org/10.1126/sciadv.adl4741
Fayolle M, Lainey V, Dirkx D, Gurvits LI, Cimo G, Bolton SJ (2023) Spacecraft VLBI tracking to enhance stellar occultations astrometry of planetary satellites. Astron Astrophys 676:L6. https://doi.org/10.1051/0004-6361/202347019
Gao P, Stevenson DJ (2013) Nonhydrostatic effects and the determination of icy satellites' moment of inertia. Icarus 226(2):1185–1191. https://doi.org/10.1016/j.icarus.2013.07.034
Garcia PA, Keszthelyi LP, Becker TB, Becker K, Sides S (2015) The present and future of pattern matching in the Integrated Software for Imagers and Spectrometers (ISIS). Lunar Planet Sci Conf 42:#2782
Gomez Casajus L, Zannoni M, Modenini D, Tortora P, Nimmo F, Van Hoolst T, et al (2021) Updated Europa gravity field and interior structure from a reanalysis of Galileo tracking data. Icarus 358:114187. https://doi.org/10.1016/j.icarus.2020.114187
Goossens S, Genova A, James PB, Mazarico E (2022) Estimation of crust and lithospheric properties for Mercury from high-resolution gravity and topography. Planet Sci J 3(6):145. https://doi.org/10.3847/PSJ/ac703f
Greenberg R, Weidenschilling SJ (1984) How fast do Galilean satellites spin? Icarus 58(2). https://doi.org/10.1016/0019-1035(84)90038-1
Hay HCFC, Fenty I, Pappalardo RT, Nakayama Y (2023) Turbulent drag at the ice-ocean interface of Europa in simulations of rotating convection: implications for nonsynchronous rotation of the ice shell. J Geophys Res Planets 128:e2022JE007648. https://doi.org/10.1029/2022JE007648
Hemingway DJ, Mittal T (2019) Enceladus's ice shell structure as a window on internal heat production. Icarus 332:111–131. https://doi.org/10.1016/j.icarus.2019.03.011
Hoppa GV, Greenberg R, Geissler P, Tufts BR, Plassmann J, Durda DD (1999) Rotation of Europa: constraints from terminator and limb positions. Icarus 137(2):341–347. https://doi.org/10.1006/icar.1998.6065
Hoppa GV, Tufts BR, Greenberg R, Hurford TA, O'Brien DP, Geissler PE (2001) Europa's rate of rotation derived from the tectonic sequence in the Astypalaea region. Icarus 153(1):208–213. https://doi.org/10.1006/icar.2001.6663
Hussmann H, Shoji D, Steinbrügge G, et al (2016) Constraints on dissipation in the deep interiors of Ganymede and Europa from tidal phase-lags. Celest Mech Dyn Astron 126:131–144. https://doi.org/10.1007/s10569-016-9721-0
Iess L, Stevenson DJ, Parisi M, Hemingway D, Jacobson RA, Lunine JI, Nimmo F, et al (2014) The gravity field and interior structure of Enceladus. Science 344(6179):78–80. https://doi.org/10.1126/science.1250551
Jacobson RA, Haw RJ, McElrath TP, Antreasian PG (2000) A comprehensive orbit reconstruction for the Galileo prime mission in the J2000 system. J Astronaut Sci 48(4):495–516. https://doi.org/10.1007/BF03546268
Kaula WM (2000) Theory of satellite geodesy: applications of satellites to geodesy (Dover ed). Dover, Mineola

Kirk RL, Howington-Kraus E, Hare TM, Jorda L (2016) The effect of illumination on stereo dtm quality: simulations in support of Europa exploration. ISPRS Ann Photogramm Remote Sens Spat Inf Sci 3:103–110

Kirk RL, Shepherd M, Sides SC (2018) A novel technique for precision geometric correction of jitter distortion for the Europa Imaging System and other rolling-shutter cameras. Int Arch Photogramm Remote Sens Spat Inf Sci XLII-3:735–739. https://doi.org/10.5194/isprs-archives-XLII-3-735-2018

Kivelson MG, Khurana KK, Russell CT, Volwerk M, Walker RJ, Zimmer C (2000) Galileo magnetometer measurements: a stronger case for a subsurface ocean at Europa. Science 289(5483):1340–1343. https://doi.org/10.1126/science.289.5483.1340

Kivelson MG, Jia X, Lee KA, et al (2023) The Europa Clipper Magnetometer. Space Sci Rev 219:48. https://doi.org/10.1007/s11214-023-00989-5

Koh Z-W, Nimmo F, Lunine JI, Mazarico E, Dombard AJ (2022) Assessing the detectability of Europa's seafloor topography from Europa Clipper's gravity data. Planet Sci J 3(8):197. https://doi.org/10.3847/PSJ/ac82aa

Kuskov OL, Kronrod VA (2005) Internal structure of Europa and Callisto. Icarus 177(2):550–569. https://doi.org/10.1016/j.icarus.2005.04.014

Lainey V, Arlot J-E Karatekin Ö, (2009) Strong tidal dissipation in Io and Jupiter from astrometric observations. Nature 459(7249):957–959. https://doi.org/10.1038/nature08108.

Lainey V, Karatekin Ö, Desmars J, Charnoz S Arlot J-E Emelyanov N Le Poncin-Lafitte C Mathis S Remus F Tobie G (2012) Strong tidal dissipation in Saturn and constraints on Enceladus' thermal state from astrometry. The Astrophysical Journal 752(1). https://doi.org/10.1088/0004-637X/752/1/14.

Lieske JH (1980) Improved ephemerides of the Galilean satellites. Astron Astrophys 82(3):340–348.

Magnanini A, Zannoni M, Casajus LG, et al (2024) Joint analysis of JUICE and Europa Clipper tracking data to study the Jovian system ephemerides and dissipative parameters. Astron Astrophys 687:A132. https://doi.org/10.1051/0004-6361/202347616

Malhotra R (1991) Tidal origin of the Laplace resonance and the resurfacing of Ganymede. Bull Am Astron Soc 23:1170. https://ui.adsabs.harvard.edu/abs/1991BAAS...23.1170M

Mazarico E, Buccino D, Castillo-Rogez J, Dombard AJ, Genova A, Hussmann H, et al (2023) The Europa Clipper gravity and radio science investigation. Space Sci Rev 219(4):30. https://doi.org/10.1007/s11214-023-00972-0

McKenzie D, Nimmo F (1997) Elastic thickness estimates for Venus from line of sight accelerations. Icarus 130(1):198–216. https://doi.org/10.1006/icar.1997.5770

Moore W, Schubert G (2000) The tidal response of Europa. Icarus 147(1):317–319. https://doi.org/10.1006/icar.2000.6460

Murray CD, Dermott SF (2000) Solar System dynamics. Cambridge University Press, Cambridge. https://doi.org/10.1017/CBO9781139174817

Neter J, Wasserman W, Kutner MH (1985) Applied linear statistical models: regression analysis of variance and experimental design 2nd edn. Richard Irwin Inc., Homewood, pp 60–70

Nimmo F, Thomas PC, Pappalardo RT, Moore WB (2007) The global shape of Europa: constraints on lateral shell thickness variations. Icarus 191(1):183–192. https://doi.org/10.1016/j.icarus.2007.04.021

Nimmo F, Bills BG, Thomas PC (2011) Geophysical implications of the long-wavelength topography of the Saturnian satellites. J Geophys Res 116:E11001. https://doi.org/10.1029/2011JE003835

Nimmo F, Umurhan O, Lisse CM, Bierson CJ, Lauer TR, Buie MW, Throop HB, Kammer JA, Roberts JH, McKinnon WB, Zangari AM, Moore JM, Stern SA, Young LA, Weaver HA, Olkin CB, Ennico K (2017) Mean radius and shape of Pluto and Charon from new horizons images. Icarus 287:12–29. https://doi.org/10.1016/j.icarus.2016.06.027

Oberst J, Zubarev A, Nadezhdina I, Shishkina L, Rambaux N (2014) The Phobos geodetic control point network and rotation model. Planet Space Sci 102:45–50. https://doi.org/10.1016/j.pss.2014.03.006

Pappalardo RT, Buratti BJ, Korth H, Senske DA, Blaney DL, Blankenship DD, Burch JL, Christensen PR, Kempf S, Kivelson MG, Mazarico E (2024) Science overview of the Europa Clipper Mission. Space Sci Rev 220(4):1–58. https://doi.org/10.1007/s11214-024-01070-5

Park RS, Jacobson RA, Gomez Casajus L, et al (2025) Io's tidal response precludes a shallow magma ocean. Nature 638:69–73. https://doi.org/10.1038/s41586-024-08442-5

Pauer M, Musiol S, Breuer D (2010) Gravity signals on Europa from silicate shell density variations. J Geophys Res 115:E12005. https://doi.org/10.1029/2010JE003595

Perry ME, Neumann GA, Phillips RJ, Barnouin OS, Smith DE, Zuber MT, Solomon SC (2015) The shape of Mercury from MESSENGER measurements. Geophys Res Lett 42(17):6951–6958. https://doi.org/10.1002/2015GL065101

Petricca F, Genova A, Castillo-Rogez JC, Styczinski MJ, Cochrane CJ, Vance SD (2023) Characterization of Icy Moon hydrospheres through joint inversion of gravity and magnetic field measurements. Geophys Res Lett 50(17):e2023GL104016. https://doi.org/10.1029/2023GL104016

Petricca F, Castillo-Rogez JC, Genova A, et al (2025) Partial differentiation of Europa and implications for the origin of materials in the Jupiter system. Nat Astron. https://doi.org/10.1038/s41550-024-02469-4
Retherford KD, Becker TM, Gladstone GR, et al (2024) Europa Ultraviolet Spectrograph (Europa-UVS). Space Sci Rev 220:89. https://doi.org/10.1007/s11214-024-01121-x
Rhoden AR, Militzer B, Huff EM, Hurford TA, Manga M, Richards MA (2010) Constraints on Europa's rotational dynamics from modeling of tidally-driven fractures. Icarus 210(2):770–784. https://doi.org/10.1016/j.icarus.2010.07.018
Roberts JH, McKinnon WB, Elder, et al (2023) Exploring the interior of Europa with the Europa Clipper. Space Sci Rev 219(6):46. https://doi.org/10.1007/s11214-023-00990-y
Seidelmann P, Abalakin VK, Bursa M, et al (2002) Report of the IAU/IAG working group on cartographic coordinates and rotational elements of the planets and satellites: 2000. Celest Mech Dyn Astron 82:83–111. https://doi.org/10.1023/A:1013939327465
Shepard MK, Campbell BA, Bulmer MH, Farr TG, Gaddis LR, Plaut J (2001) The roughness of natural terrain: a planetary and remote sensing perspective. J Geophys Res 106(EAS):32777–32795
Steinbrügge G, Schroeder DM, Haynes MS, Hussmann H, Grima C, Blankenship DD (2018) Assessing the potential for measuring Europa's tidal Love number h2 using radar sounder and topographic imager data. Earth Planet Sci Lett 482:334–341. https://doi.org/10.1016/j.epsl.2017.11.028
Steinbrügge G, Voigt J, Schroeder D, Stark A, Haynes M, Scanlan K, Hamilton C, Young D, Hussmann H, Grima C, Blankenship D (2020) The surface roughness of Europa derived from Galileo stereo images. Icarus 343:113669. https://doi.org/10.1016/j.icarus.2020.113669
Steinbrügge G, et al (2022) Altimetry measurements from planetary radar sounders and application to SHARAD on Mars. IEEE Trans Geosci Remote Sens 60:1–14. https://doi.org/10.1109/TGRS.2021.3134638. Art no. 5109214
Thomas PC, Davies ME, Colvin TR, Oberst J, Neukum G, Carr MH, McEwen A, Schubert G, Belton MJS (1998) The shape of Io from Galileo limb measurements. Icarus 135(1):175–180. https://doi.org/10.1006/icar.1998.5987
Thomas PC (2010) Sizes, shapes, and derived properties of the saturnian satellites after the Cassini nominal mission. Icarus 208(1):395–401. https://doi.org/10.1016/j.icarus.2010.01.025
Tricarico P (2014) Multi-layer hydrostatic equilibrium of planets and synchronous moons: theory and application to Ceres and to Solar System moons. Astrophys J 782(2):99. https://doi.org/10.1088/0004-637X/782/2/99
Turcotte D (1993) Fractals and chaos in geology and geophysics 1st paperback edn. Cambridge University Press, Cambridge, pp 73–94
Turtle EP, McEwen AS, Patterson GW, et al (2024) The Europa Imaging System (EIS) investigation. Space Sci Rev 220:91. https://doi.org/10.1007/s11214-024-01115-9
Van Hoolst T, Baland R-M, Trinh A (2013) On the librations and tides of large icy satellites. Icarus 226(1):299–315. https://doi.org/10.1016/j.icarus.2013.05.036
Vance SD, Craft KL, Shock E, et al (2023) Investigating Europa's habitability with the Europa Clipper. Space Sci Rev 219:81. https://doi.org/10.1007/s11214-023-01025-2
Wahr JM, Zuber MT, Smith DE, Lunine JI (2006) Tides on Europa and the thickness of Europa's icy shell. J Geophys Res Planets 111(E12):2006JE002729. https://doi.org/10.1029/2006JE002729

Authors and Affiliations

G. Steinbrügge[1] · R.S. Park[1] · J.H. Roberts[2] · M. Bland[3] · S. Brooks[1] · J. Castillo-Rogez[1] · G. Cascioli[4,5] · A. Genova[6] · T. Greathouse[7] · H. Hussmann[8] · R. Kirk[3] · A. Magnanini[9] · E. Mazarico[4] · F. Nimmo[10] · M.S. Park[11] · F. Petricca[1] · K. Retherford[7] · D.M. Schroeder[12] · K.M. Soderlund[13] · P. Tortora[9] · M. Zannoni[9]

✉ G. Steinbrügge
gregor.b.steinbruegge@jpl.nasa.gov

[1] Jet Propulsion Laboratory, California Institute of Technology, Pasadena, CA, USA

[2] Johns Hopkins Applied Physics Laboratory, Laurel, MD, USA

[3] United States Geological Survey, Flagstaff, AZ, USA

[4] NASA Goddard Space Flight Center, Greenbelt, MD, USA

[5] Center for Space Sciences and Technology, University of Maryland Baltimore County, Baltimore, MD, USA

[6] Sapienza University of Rome, Rome, Italy

[7] Southwest Research Institute, San Antonio, TX, USA

[8] Institute of Space Research, German Aerospace Center, Berlin, Germany

[9] Alma Mater Studiorum – University of Bologna, Forlì (FC), Italy

[10] University of California, Santa Cruz, CA, USA

[11] Department of Geophysics, Stanford University, Stanford, CA, USA

[12] Institute for Computational and Mathematical Engineering, Stanford University, Stanford, CA, USA

[13] University of Texas at Austin, Austin, TX, USA